THE LASER HEATER SYSTEM OF SWISSFEL

M. Pedrozzi, M. Calvi, R. Ischebeck, S. Reiche, C. Vicario, PSI, Villigen, Switzerland

B. D. Fell, N. Thompson, STFC/DL/ASTeC, Daresbury, UK

Abstract

Short wavelength FELs are generally driven by high-brilliance photo-cathode RF-guns which generate electron beams with an uncorrelated energy spread on the order of 1 keV or less. These extremely cold beams can easily develop micro-bunching instabilities caused by longitudinal space charge forces after the compression process. This can result in a blow up of the energy spread and emittance beyond the tolerable level for SASE emission. It has been demonstrated theoretically and experimentally [1] that a controlled increase of the uncorrelated energy spread to typically a few keV is sufficient to strongly reduce the instability growth. In the laser heater system, one achieves a controlled increase of the beam energy spread by a resonant interaction of the electron beam with a transversally polarized laser beam inside of an undulator magnet. The momentum modulation resulting from the energy exchange within the undulator is consequently smeared out in the transmission line downstream of the laser heater system. In SwissFEL, the laser heater system is located after the first two S-band accelerating structures at a beam energy of 150 MeV. This paper describes the layout and the sub-components of this system.

INTRODUCTION

SwissFEL is the hard X-ray free-electron laser presently under construction at PSI in Switzerland [2-3]. Table 1 summarizes the main beam parameters at the injection in the undulator section specified for SASE operation at 1 Å radiation.

Table 1: Beam Parameters - SASE Hard X-Ray Line

Parameter		units
Energy	5.8	GeV
Charge	200/10	pC
Uncorrelated RMS slice energy spread	350/250	keV
RMS normalized projected emittance	< 0.65/0.25	mm.mrad
RMS normalized slice emittance	<0.43/0.18	mm.mrad
Peak current	2.7/0.7	kA
Bunch length	25/6	fs

The final electron beam energy of roughly 6 GeV was defined according to the state of the art accelerator and undulator technology in order to maximize compactness and minimize costs. The energy is relatively low with respect to other facilities of this class resulting in tighter beam quality requirements. The mitigation of emittance and energy spread growth during the acceleration and compression of the electron beam, caused in particular by micro-bunching instabilities [4-5], are therefore of primary importance for this facility [6]. It should be noted that for efficient self-seeding operation one aims to reach a normalized slice emittance of ~0.3 mm.mrad. The SwissFEL injector complex includes a laser heater (LH) system which will allows a controlled enhancement of the uncorrelated energy spread of the electron beam. Carefully adjusted, the energy spread can drastically reduce the gain of the micro-bunching instability without affecting the FEL performances.

SYSTEM DESCRIPTION

General Layout

Figure 1 shows a schematic of the SwissFEL injector facility. The PSI RF Photo-injector [7] produces 7.1 MeV high brightness electron bunches with an intrinsic emittance of 0.55 mm.mrad/mm [8] and a peak current of 20 A. The normalized slice emittance at the end of the injector with uncompressed beam will be typically around 0.2 mm.mrad for a bunch charge of 200 pC [9]. In Booster 1 two S-band traveling-wave cavities accelerate on crest the electron beam up to 150 MeV. After this first acceleration stage a set of 5 quadrupoles allows matching the optical functions trough the laser heater chicane and 5 additional quadrupoles follow the LH modulator undulator to control the matching in booster 2. This section consists of two S-Band RF modules including each one klystron amplifier and two accelerating cavities. In booster 2 one accelerates off crest (up to 345 MeV) to provide the necessary energy-time correlation needed for the compression. Enough space has been reserved to allow future energy upgrades with a third RF accelerating module. The focusing along booster 2 consists of three FODO cells with 11m period. To suppress the second order energy-time correlation two X-band RF cavities (S-band 4th harmonic) running in decelerating mode precede the 13.5 m long compression chicane which is typically operated at compression factors between 10 and 15. The final nominal energy of the injector is 320 MeV.

Laser Heater Basic Specifications and Layout

As schematically illustrated in Figure 2 the LH consists of 3 main parts:

- A small magnetic chicane required for the laser coupling which corresponds to the first dispersive section of the accelerator complex.
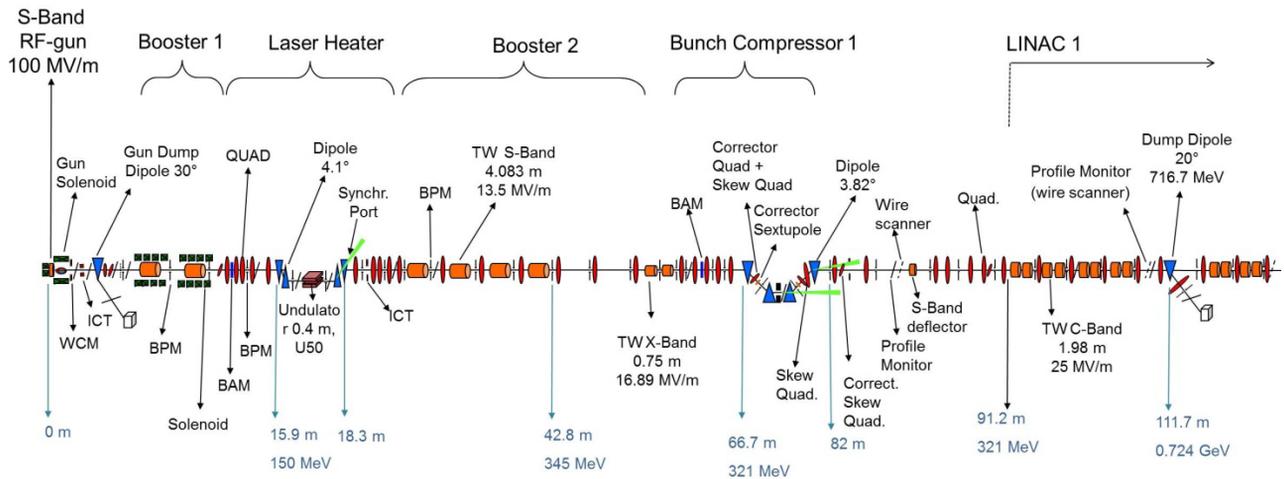
Figure 1: SwissFEL injector facility, schematic layout.

- An undulator modulator to allow a resonant energy exchange between laser and electron beam.
- The diagnostics elements for setting and monitoring the laser-beam overlap.
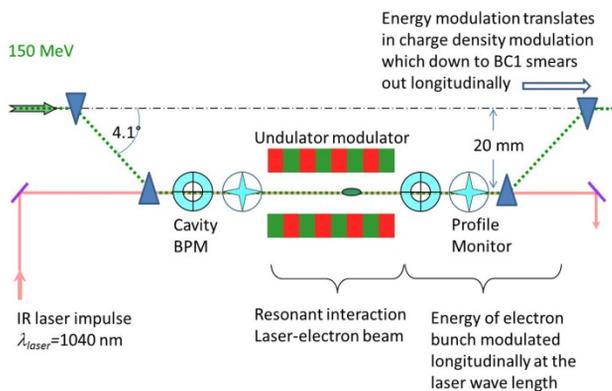

Figure 2: Laser heater basic principle.

The basic parameter of chicane, electron beam and laser are reported in table 2. The relatively low R56 was chosen in order to facilitate the matching for testing alternative compression schemes at low energy with velocity bunching.

The nominal electron beam energy was set as high as possible to allow an efficient power distribution between RF plants without compromising the emittance compensation process and keeping a safety margin on the RF power plants. The laser wavelength is defined by the Yb:CaF$_2$ photo cathode laser system. The choice of this technology is mainly driven by stability consideration. As described later in this paper, a fraction of the IR radiation produced by this system is used for the LH system.

Mechanically the LH beam line sits on three independent support girders as illustrated in Figure 3. At the entrance of the LH section a Beam Arrival Monitor (BAM) [10] delivers precise measurements of longitudinal drifts and jitter of the electron beam. During operation this tool helps surveying and maintaining the longitudinal laser-beam overlap.

Table 2: Laser Heater Parameters

Beam parameters		
Charge (pC)	10	200
Beta function @ undulator X/Y (m)	42 / 18	42/18
Proj. norm. emittance (mm.mrad)	0.15	0.3
RMS beam size (µm)	146	207
Nominal energy (MeV)	150 ± 1.5 %	
Pulse length flat top (ps)	10	3
Chicane dispersion (mm)	20.14	
Chicane parameters		
Bend angle (deg)	4.1	
Dipole 1/3 & 3/4 separation (mm)	280	
Dipole 2-3 separation (m)	1.82	
Dipole yoke length (mm)	120	
Off axis separation (mm)	20	
R56 (mm)	2.4	
Laser main parameters		
Wavelength (nm)	1040	
FWHM pulse lengths (ps)	50	
Waist at Focus (µm)	400	
Max. laser energy at LH (µJ)	100	

The undulator modulator and the magnetic chicane sit on the central girder. Two diagnostic modules consisting of one BPM followed by a screen are located upstream and downstream the undulator. Standard SwissFEL cavity BPMs and screens with chamber aperture of 16 mm are used. These monitors are required for adjusting and monitoring the transverse laser-beam overlap. As shown
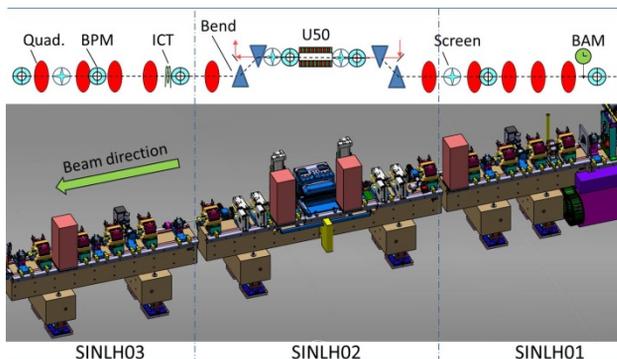
Figure 3: 3D Model of the LH beam line with schematic description of the main components.

in Figure 4 the central section of the chicane vacuum chamber, including screens and BPMs, is movable allowing a straight orbit with dipole OFF and with 20 mm off axis operation. Additionally the undulator can be remotely retracted from its nominal position by 100 mm to become invisible for the beam.
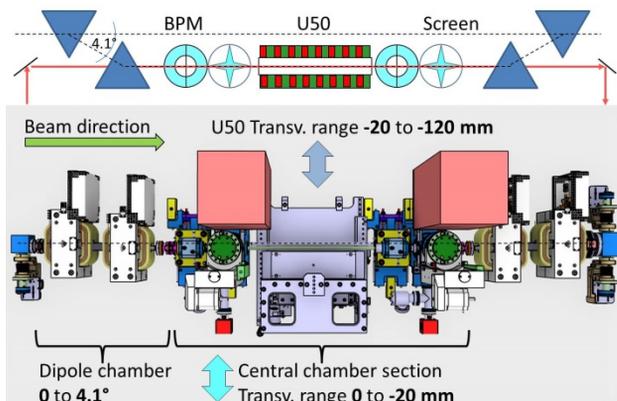

Figure 4: Movable parts in the LH chicane, with undulator in retracted position and chicane at 4.1°.

Laser System and Transfer Line

An infrared Yb-CaF$_2$ laser amplifier from the company Amplitude Système (Bordeaux) is used to generate by frequency multiplication the UV radiation for the RF-gun photocathode while the fundamental wavelength is used to drive the LH system. Figure 5 shows a schematic layout of the laser components that will be located in the SwissFEL laser room sitting alongside the accelerator tunnel near the gun region.
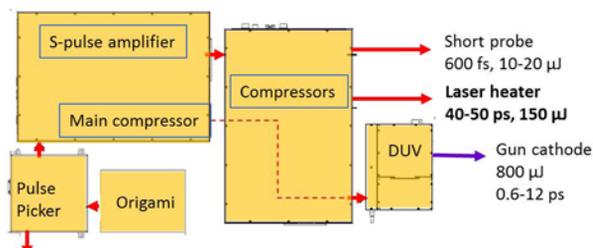

Figure 5: Layout of the laser system.

With a typical FWHM pulse length of 50 ps, the nominal operation of the LH would require moderate laser energy up to ~1.1 µJ (22 kW). For diagnostic purposes the system can deliver up to 150 µJ at the source which should correspond to 100 µJ (2 MW) at the LH undulator modulator. Driving the resonant interaction with laser powers between 200 kW and 2 MW should allow a fine adjustment of the longitudinal overlap by observing a broadening of the electron beam energy spread between 20 and 65 keV. The energy spectrometer can typically resolve a couple of keV.
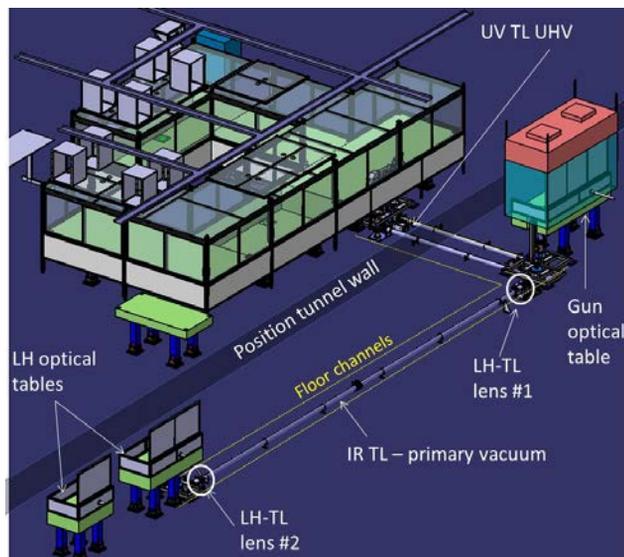

Figure 6: 3D model of the laser infrastructure with hidden accelerator components and building elements.

An independent in vacuum Transfer Line (TL) sitting in a floor channel assures the transport of the beam from the laser room down to the LH as shown in Figure 6. All mirrors of the TL are motorized and sit on supports directly fixed on the concrete floor and decoupled from the vacuum chamber to minimize pointing jitter due to vibrations. As shown in Figure 7 two lenses in the TL are used to image the laser beam from the laser room and to minimize the beam displacement due to laser angular jitter to few µm.
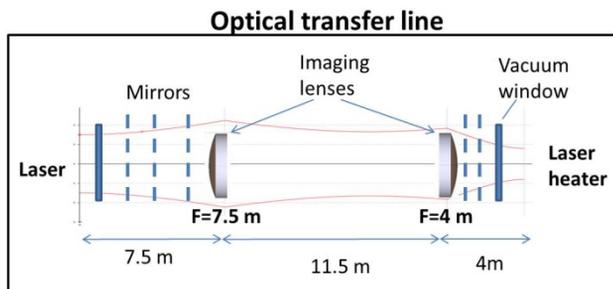

Figure 7: Schematic of the laser transfer line.

On the laser heater table (Figure 8) a set of motorized mirrors and a variable telescope are used to control the position and the beam size of the laser for optimal overlap with the electron beam. A variable attenuator will be used

to continuously adjust the laser energy. Finally a motorized delay stage will control the laser arrival time at the laser heater.

Electron and Laser Diagnostic Systems

The main functionalities to be investigated while designing the diagnostic system are:

- Adjustment: setting of the transverse and longitudinal laser-electron beam overlap
- Operation: monitoring of laser and electron beam parameters, and in particularly feedback on the longitudinal and transverse Overlap

Multiple laser heater diagnostics are needed to address the two above functionalities. Offline energy meters and online calibrated photodiodes will monitor the laser pulse energy at different locations. A camera system movable along a "virtual undulator" will record the laser beam shape and size. Cromox screens are suited as common in vacuum profile monitors for laser and electron beam to adjust the transverse overlap. Position sensitive detectors will be installed on the input and output optical laser heater table for precise laser alignment in the undulator. These sensors, in combination with the BPM placed in front and after the undulator, will allow surveying the transverse overlap during operation. For rough longitudinal synchronization, the laser arrival time will be measured with few tens ps resolution using a fast photodiode and a large bandwidth oscilloscope. For fine adjustment of the longitudinal overlap the LH will be overdriven up to ~2 MW laser power. At this intensity level the uncorrelated energy spread will be approximately ~65 keV, which should easily measurable in the energy spectrometer at 320 MeV. Since we do not expect large longitudinal fluctuation of the laser system, the BAM measurements of electron arrival should suffice for monitoring the longitudinal overlap during operation.

Figure 8: Schematic layout of diagnostic and control instrumentation.

Undulator System

The SwissFEL LH undulator is a planar permanent magnet Halbach array with 8 full periods of period length λ_u=50mm. The magnetic structure is longitudinally antisymmetric (the longitudinal centre of the undulator coincides with a zero crossing of the vertical magnetic field) so that the electron trajectory is centred on the magnetic axis. Table 3 summarizes the parameters of the magnetic blocks while Figure 9 shows the characteristic block shape.

Table 3: Properties of the Magnet Blocks

66 full length blocks (12.35 mm)	
Material	NdFeB
Grade	VACODYM 863 TP
Remanent field	1.25 T
Magnetisation	34 in +z, 32 in +y
Field tolerance	1%
Magnetisation angle tolerance	± 1 deg
12 end blocks	
Length 9.26mm ±25µm	4 magnetized +y
Length 6.18mm ±25µm	4 magnetized +z
Length 3.24mm ±25µm	4 magnetized +y

The undulator has been modelled in RADIA [11]. The computed variation of peak K versus full gap is shown in Figure 10. At gap 20mm (full closed), $K = 2.54$, and at gap 40mm (full open), $K = 0.667$.
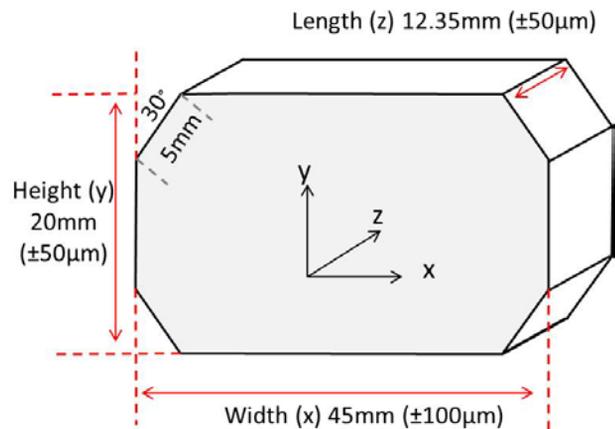

Figure 9: Shape of the magnetic blocks.

The undulator strength and period are linked to the laser wavelength and the beam energy via the resonance relation:
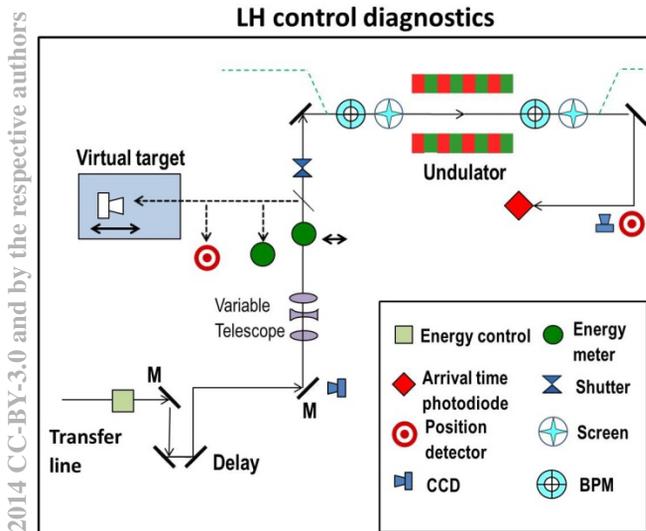
$$\lambda_{laser} = \frac{\lambda_u}{2\gamma^2}\left(1 + \frac{K^2}{2}\right)$$

$$K = \frac{eB_0\lambda_u}{2\pi m_e c} \tag{1}$$

where λ_u is the undulator period and K the undulator parameter. At the nominal energy of 150 MeV the resonance condition requires K=2.28 which corresponds to a gap of approximately 22 mm but the tuning range of the undulator allows operating the LH at energies ranging from 87 to 162 MeV.
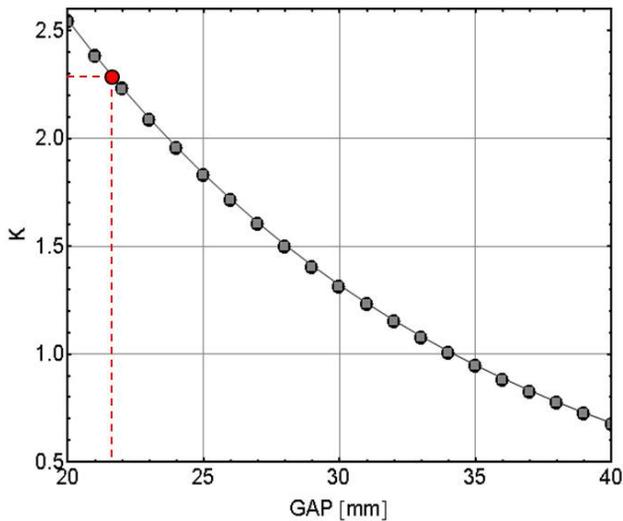

Figure 10: Tuning range of the U50 undulator factor K versus gap. In read the nominal K for 150 MeV.

Figure 11 shows calculated horizontal and vertical good field regions ($\Delta K/K_0 \leq 10^{-4}$) versus the undulator parameter K. At the nominal K the expected good field region are respectively ~620 and ~150 µm. These values determine the alignment tolerances of the electron bunch orbit along the undulator.
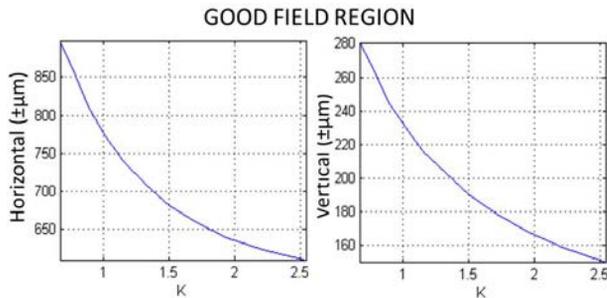

Figure 11: Horizontal and Vertical good field regions ($\Delta K/K0 \leq 10^{-4}$) versus K.

STFC/ASTeC is in charge of the design, engineering and mechanical realization of the undulator assembly. Figure 12 shows the undulator during the assembly phase in the workshop at Daresbury Laboratory and the 3D model of the device mounted on the girder.

To set the exit position of a 150MeV beam exactly on axis (or to minimise the field 2nd integral) the end 1/4 length blocks are increased in length by 150µm. Because the design is antisymmetric the 1st integral (hence exit angle) is automatically zero for all gaps.

The specification for on-axis field quality is that the maximum relative variation in K is 1% rms. This is calculated from the maximum positive and negative B_z for each period, so is an average of 16 data points. The tolerances on block dimensions, field strength and field angle have then been specified so that the average of a set of unshimmed, perfectly constructed undulators, with errors added to each randomly in a uniform distribution, is within specification by factor of two, and all the unshimmed random undulators satisfy the specification.

Figure 12: U50 during assembly at Daresbury Laboratory and 3D model of the undulator on the support girder in extracted position.

BEAM DYNAMICS CONSIDERATIONS

Energy Spread Enhancement and FEL Operation

The final rms slice energy spread at the FEL undulator line scales proportionally to the compression factor with the uncorrelated energy spread after the LH. To avoid diluting the FEL performances, the relative energy spread must stay below the relative Bandwidths (BW) of the FEL. When operating SwissFEL at 5.8 GeV, and with the characteristic SwissFEL BW of 0.05% (corresponding to 2.9 MeV) one can tolerate at best ~1MeV energy spread before starting to degrade the FEL efficiency. With a compression factor of 150, this value corresponds to a maximum tolerable uncorrelated energy spread after the LH of ~7 keV. Running a few simulations with ASTRA from the gun up to the end of booster 1 and then ELEGANT in the LH section using the "laser modulator" element and assuming a laser waist of 400 µm one finds the approximate scaling relation between laser intensity and uncorrelated energy spread after the LH as:

$$\sigma_E(keV) \approx \sqrt{2.15 P_{laser}(kW)} \tag{2}$$

Figure 13 illustrated the energy spread dependency described by equation (2) in the region of interest for the nominal operation of the LH up to a level compatible for overlap diagnose purposes.

As anticipated in this paper, a nominal laser power up to 22 kW should be sufficient to drive the LH at its nominal operation point. It should be noted that the LCLS measurements [1] show a weak FEL power dependency versus the laser intensity around the optimum operating point, relaxing the amplitude jitter tolerances of the IR laser source.
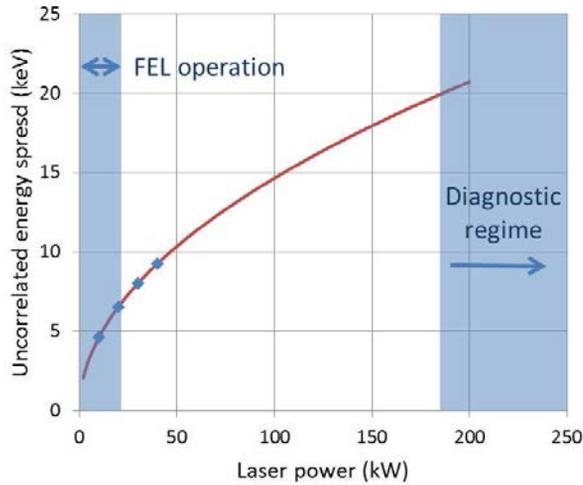

Figure 13: RMS uncorrelated energy spread versus Laser power. Blue dots from Elegant simulations assuming 150 MeV, 1040 nm laser wavelength, 400 µm laser waist, read equation 2.

Consideration on Trickle Heating

At LCLS an unexpected increase of the electron heating after the LH was clearly observed for very low laser powers. While the 1 D theory predicts negligible contributions of the Longitudinal Space Charge (LSC) to the energy spread growth, Z. Huang demonstrated the 3D nature of the observed phenomenon occurring when tilted µ-bunches are transported after the LH chicane applying strong horizontal focusing [1]. Basically the x-s density modulation doesn't smear completely after the half LH chicane but remains hidden in the x'-s plane. After a 90 deg phase advance this correlations develops again in x-s which, if associated with strong focusing, can considerably enhance the contribution of LSC. In SwissFEL the phase advance from the LH down to the first accelerating cavity of booster 2 is only 23° (see Figure 14) while the beta function remains relatively large (>10m) getting smaller only at the entrance of the linac where the energy rapidly boosts up.

In LCLS the beam propagate 11 m before injection in the next accelerating cavity experiencing phase advances larger than 90°. In SwissFEL this distance is only 2.5 m.

Figure 15 shows the longitudinal slice phase space at three different locations between the exit of the LH chicane and the first accelerating structure of Booster 2. From these measurements one can deduce the correlation factor R and evaluate the 3D electric field enhancement of LSC with respect to the 1D theory given by the following relation:
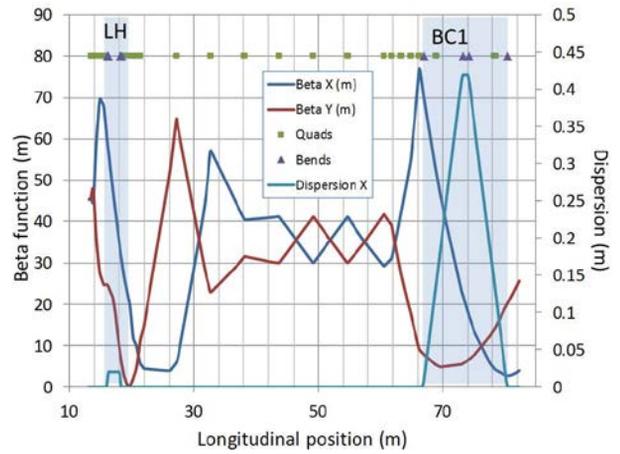
Figure 14: SwissFEL injector optics from the LH section up to the first bunch compressor.
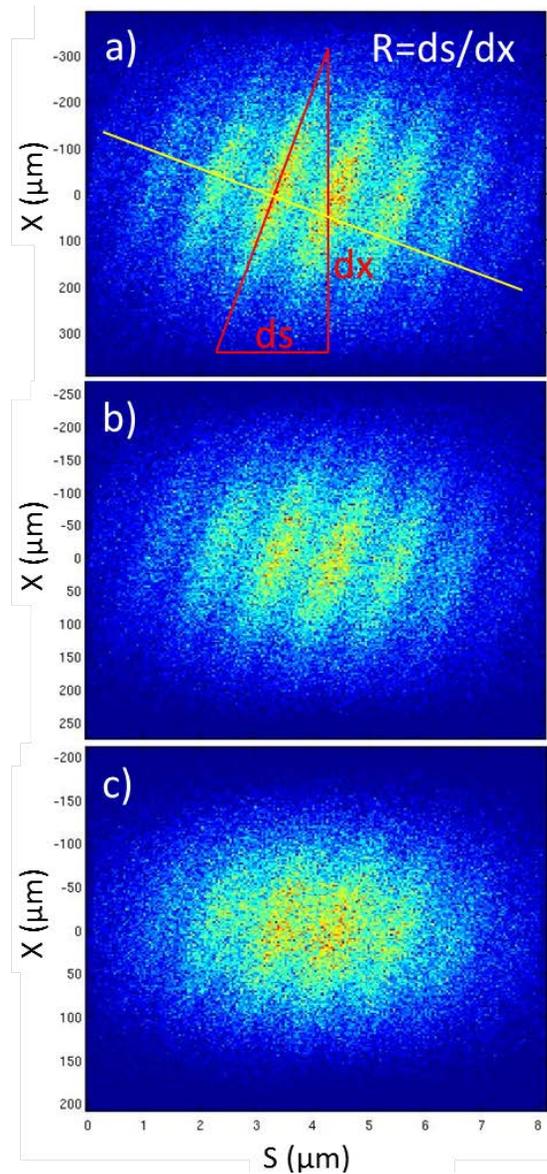

Figure 15: x-s phase space at a) 19.21 m, b) 20.46 m and c) 21.59 m.

$$\frac{E_k^{3D}}{E_k^{1D}} = \frac{e^{k^2 R^2 \sigma_x^2 / 2}}{1 + \gamma^2 R^2} \qquad (3)$$

where $k = 2\pi/\lambda_{laser}$, R the correlation factor, σ_x the horizontal rms beam size and γ the Lorenz factor.

Table 4: LSC Enhancement after the LH Chicane

S (m)	$\sigma_x(\mu m)$	R	LCS
19.21	153	0.00325	48
20.46	101	0.0046	18.5
21.59	71	0.0058	5.6

Table 4 summarizes the LSC enhancement in the case of SwissFEL at the location described in Figure 15 assuming 150 MeV beam energy and 1040 nm laser wavelength. Directly at the LH exit the enhancement factor is approximately 50 but it rapidly drops toward booster 2.

One can notice that these values are consistently lower than the enhancement factor of ~250 estimated for the LCLS in [1]. It should be noted in addition that the relaxed optic following the LH section allows maintaining the bunching factor predicted by the 3D theory well below his maximum preventing over-bunching as observed with the nominal optic at LCLS.

CONCLUSION

The SwissFEL baseline layout incudes a Laser Heater system placed at 150 MeV. This system allows a controlled increase of the uncorrelated energy spread to fight micro-bunching instabilities possibly developing in the compression stages of the accelerator. The tuning range of the 50 mm period undulator allows in principle operating the LH beam for energies ranging from 87 up to 162 MeV, well matching the operational range of the accelerating cavities in booster 1. The LH system can be made completely invisible to the beam by extracting the undulator to an off axis position. The relaxed optic functions in the short transport line after the LH should efficiently cope with trickle heating at the nominal operational conditions of the laser heater.

REFERENCES

[1] Z. Huang, et al., Measurements of the coherent light source laser heater and its impact on the x-ray free-electron laser performance, Phys. Rev. Special Topics – Accelerator and beams 13, 020703 (2010).

[2] SwissFEL Conceptual Design Report, Paul Scherrer Institut, Villigen, Switzerland, Report: 10-04.

[3] H. H. Braun, in Proc. 34th Int. Free-Electron Laser Conf., Nara, Japan, 2012, pp. 9-12.

[4] M. Borland, Coherent Synchrotron Radiation And Microbunching In Bunch Compressors, in Proc. 21st Int. Linac Conference, Gyeongju, Korea, pp. 11-15, 2002.

[5] Z. Hunag et al., Microbunching Instability due to Bunch Compression, ICFA Beam Dynamics Newsletter No. 38, 2005, pp. 37-51.

[6] S. Bettoni et al., Microbunching Instability Studies In SwissFEL, in Proc. 2nd Int. Particle Accelerator Conf. New Orleans, Louisiana, USA, 2012, pp. 1744-1746.

[7] J.-Y. Raguin et al., The SwissFEL RF Gun: Design and Thermal Analysis, in Proc. 26th Linac Conference, Tel-Aviv, Israel, 2012, pp. 442-444.

[8] E. Prat, et al., Thermal Emittance Measurements at the SwissFEL Injector Test Facility, in These Proceedings: Proc. 36th Int. Free-Electron Laser Conf., Basel, Switzerland, 2014, THC02.

[9] E. Prat, et al., Slice Emittance Optimization at the SwissFEL Injector Test Facility, in Proc, 35th Free-Electron Laser Int. Conf, New York, 2013, pp. 200-204.

[10] V. Arsov, et al., First Results from the Bunch Arrival-Time Monitor at the SwissFEL Test Injector, in Proc. 2nd Int. Beam Instrumentation Conf., Oxford, UK, 2013, pp. 8-11.

[11] P. Elleaume, et al., Computing 3D Magnetic Fields From Insertion Devices, in Proc. 17th Particle Accelerator Conference, Vancouver, 1997, pp. 3509-3511.